Hindawi
Advances in Civil Engineering
Volume 2022, Article ID 7221168, 10 pages
https://doi.org/10.1155/2022/7221168

Research Article

Numerical Simulation of Coupling Support for High-Stress Fractured Soft Rock Roadway in Deep Mine

Wenhua Yuan, Ke Hong, Run Liu, Lianjie Ji, and Long Meng

School of Civil Engineering and Architecture, Anhui University of Science and Technology, Huainan, Anhui 232001, China

Correspondence should be addressed to Wenhua Yuan; whyuan@aust.edu.cn

Received 24 January 2022; Revised 26 April 2022; Accepted 27 April 2022; Published 17 May 2022

Academic Editor: Xingxin Chen

Aiming at the difficulties during the support of high-stress fractured soft rock roadway in deep mine, a comprehensive surrounding rock management method of bolt-net-cable-grout coupling support is proposed and the mechanism of interaction between coupling support and surrounding rock is analyzed by numerical simulation. The effectiveness of the coupling support is proved by an application in the east wing return-air roadway in the Qingdong Coal Mine of Huaibei Mining Group. The results show that the surrounding rock plastic zone near the sidewall and floor of high-stress fractured soft rock roadway is larger than that near the roadway roof, and its distribution range can be reduced by using the coupling support. And, the coupling support can improve the reliability of roadway support and the stability of surrounding rock by reducing the axial stress of anchor bolts, the stress concentration of surrounding rock caused by anchor bolt, the roadway surface displacement, and deep displacement of surrounding rock.

1. Introduction

There are about 73.2% of China's coal reserves are buried below 600 m. With the increase of energy demand and the decrease of shallow coal resources, the mining industry has gradually entered into the stage of deep energy exploitation [1]. However, the increasing depth of coal mining brings frequent engineering disasters, such as rock burst, gas explosion, large deformation, high ground temperature, and others, which seriously threaten the safe and efficient exploitation of deep coal resources. Therefore, the rock mechanics and support in deep resource mining have always been one of the research hotspots in the industry [2–4]. Under the influence of high in situ stress, the deep rock mass is in a state of high compressive deformation or failure limit and its mechanical properties are obviously different from shallow rock mass. In deep strata, the disturbance and failure of surrounding rock caused by excavation lead to large deformation and support difficulties of roadway and seriously threaten the safe production of coal mines [5–10].

Fault fracture zone is a common adverse geological phenomenon during roadway excavation, and its distribution area is one of the unstable sections of surrounding rock. The problems ubiquitous in the fault fracture zone, including high stress concentration, poor self-stability of fissured surrounding rock, and easy collapse of surrounding rock, often lead to geological disasters such as roof collapse and water inrush during excavation of roadway.

The high-stress fractured soft rock roadway is threatened by both the high in situ stress and the fault fracture zone mentioned above, and its support technology needs to be proposed and improved. In fact, in order to effectively control the large deformation of high-stress fractured soft rock roadway in a deep mine, researchers and technicians have carried out some studies and put forward some control techniques. By analyzing the deformation reasons of deep high-stress soft rock roadway, Yang et al. [11] proposed a combined supporting technology to coordinate nonuniform deformation of surrounding rock, control squeeze flow of floor heave, and strengthen the bearing structure of the surrounding rock. Chen et al. [12] put forward an innovative "relief-retaining" control technology of floor heave, which is a comprehensive measure that is composed of cutting groove in the floor, drilling for pressure relief at the roadway

side, and setting retaining piles at the junction of roadway side and floor. Based on numerical simulation, Zheng et al. [13] improved the bearing structure of support and proposed a high-strength combined support system with higher integrity and bearing capacity, which is consisted of cable bolt, fiber-reinforced shotcrete, steel mesh, split sets, resin bolt, and cement grouting. Wang et al. [14] proposed a double-shell grouting technology with low-pressure grouting and high-pressure split grouting to improve the overall mechanical properties of the surrounding coal and rock mass and prevent the large deformation and failure of the roadway. Meng et al. [15] adopted the finite difference program FLAC3D to analyze the distribution characteristics of supporting stress induced by bolt and anchor cable under different conditions of pretightening force and inter-row distance. Jiang et al. [16] analyzed the characteristics of rock large deformation and bolting component failure under different methods of support and put forward a support technology of the bolting, U-shaped yielding steel arches and back filling in synergy, which provided an effective measure for the soft rock roadway control in 1000 m or more deep coal mines. He et al. [17] proposed the bolt-mesh-anchor coupling support technology for the floor heave of deep coal roadway, which effectively controlled the large deformation and floor heave of deep coal roadway. By analyzing the stress environment and failure mechanism of the surrounding rock, Xu and Wei [18] put forward the combined control technology of "prestressed grouting anchor cable + grouting anchor bolt + grouting behind the wall + floor reconstruction" to control the occurrence of roadway floor heave.

By combining numerical simulation with the field test, this paper studies the deformation mechanism of high-stress fractured soft rock roadway then puts forward the joint reinforcement plan of bolt-net-cable-grout coupling support.

2. Project Overview

East wing return-air roadway is located in the seventh mining area near the BF2 fault in the Qingdong Coal Mine of Huaibei Mining Group, to its east is the east wing transport roadway and to its west is the 854 working face. The roadway has an altitude between −630 m to −629 m, and it passes through No.8 coal seam, No.7 coal seam, and No.5 coal seam, siltstone, aluminous mudstone, and mudstone. The inclination direction of coal and rock seam ranges from 30° to 48°, and the dip angle is about 12°. The east wing return-air roadway is in the influence area of the BF2 fault. The BF2 fault is a normal boundary fault between the 5th mining area and 7th mining area, with an NE strike, a dip angle of 55° to 70°, and a height from 70 m to 170 m. The BF2 fault has a long extension and suffers obvious tectonic stress. According to the in situ stress test results, the in situ stress field of the roadway is mainly tectonic stress and the principal stress is distributed horizontally. The horizontal stress component in the north-south direction is large, which is 15.9 MPa. The above-given information indicates that the roadway is a typical high-stress fractured soft rock roadway.

3. Parameters of Bolt-Net-Cable-Grout Coupling Support

The traditional roadway support generally composed of bolt-mesh, and steel belts cannot meet the support needs of the high-stress fractured soft rock roadway. The excavation of the east wing return-air roadway proved the above-mentioned viewpoint because the BF2 fault and high in situ stress caused a series of problems in the roadway with traditional support, such as the roof fracture and separation, the sinking of mesh bag and top roof, the large deformation of roadway, and the floor heave. Obviously, a new type of support is needed to be proposed to solve the problem of high-stress fractured soft rock roadway.

In order to effectively control the deformation and damage of high-stress fractured soft rock roadway, a new two-step coupling support technology is proposed, which is composed with "bolt + net + steel belt + shotcrete + cable + grout." The two-step can be described as the primary support and secondary support. The new coupling support is first used in the east wing return-air roadway, as shown in Figure 1, to try to solve the problems existing.

3.1. Primary Support. The primary support adopts a coupling support of "blot + net + shotcrete + cable + roof and side grout" with the following parameters.

3.1.1. Anchor Bolt. High-strength screw-thread steel bolt ($\Phi 22 \times 2600$ mm) is adopted with a spacing of 800×800 mm and 13 bolts in each row. An anchor bolt is used along with the JSMZ20-22 new bolting device. The new bolting device has a spacing of 1600×1600 mm with 5 devices in each row. Each bolt is anchored with 2 rolls of Z2550 resin anchor agent. The size of the bolt tray is $200 \times 200 \times 10$ mm.

3.1.2. Anchor Cable. A hollow grouting anchor cable ($\Phi 21.6 \times 7000$ mm) is used with a spacing of 1600×3200 mm and 3 cables in each row. All of the cables are used along with the JSMZ20-22 new bolting device. The anchor cable tray is a special tray with a size of $300 \times 300 \times 16$ mm. Each anchor cable is anchored with 3 rolls of Z2550 type resin anchor agent.

3.1.3. Net. Reinforcing steel mesh ($\Phi 6 \times 2500 \times 900$ mm) is used with a grid of 100×100 mm and lap length of 100 mm. Reinforcing steel mesh is laid in full section and hooked or tied with double strands of no less than 14# iron wire in a spacing of 200 mm.

3.1.4. Shotcrete. P.O 42.5 cement, sand with a particle size greater than 0.35 mm, stone with a particle size between 5 mm and 10 mm, and J85 accelerating agent are chosen as mixing materials. The mass ratio of cement, sand, stone, and the accelerating agent is 1 : 2 : 2 : 0.04. The prepared shotcrete has a strength of C20 and a thickness of 50 mm.

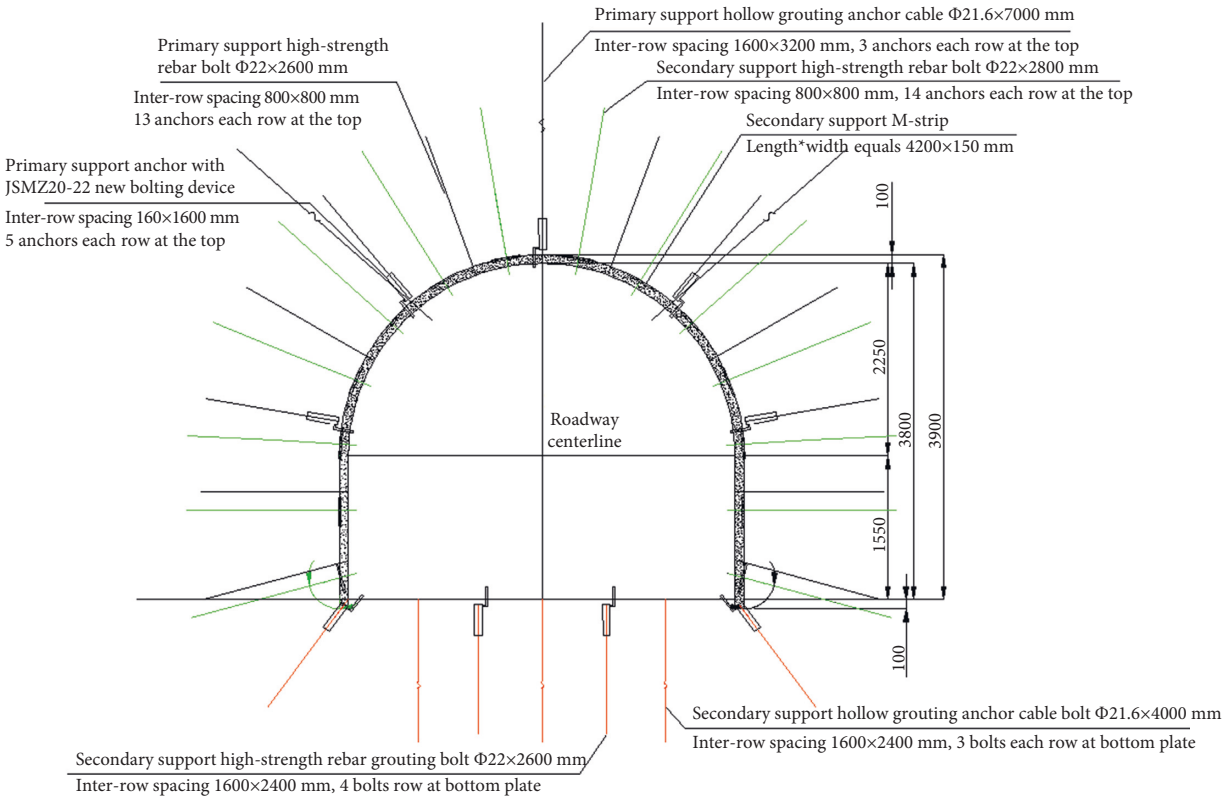

Figure 1: Full-section of bolt-net-cable-grout coupling support.

3.2. Secondary Support. Secondary support adopts a coupling support of "bolt + net + shotcrete + steel belt + floor grout."

3.2.1. Anchor Bolt. High-strength screw-thread steel bolt (Φ22 × 2800 mm) is adopted, with a spacing of 800 × 800 mm and 14 bolts in each row. Each bolt is anchored with 2 rolls of Z2550 resin anchor agent. A special tray for the M-mode steel belt is used.

3.2.2. Steel Belt. M-mode steel belt with a length of 4200 mm and width of 150 mm is arranged along the roadway direction.

3.2.3. Net. Reinforcing steel mesh for the secondary support is the same as that for the primary support.

3.2.4. Shotcrete. The secondary support has the same mix proportion of shotcrete as the primary shotcrete. But the thickness of shotcrete is 70 mm for the secondary support.

3.2.5. Floor Anchor Bolt. High-strength screw-thread steel bolt (Φ22 × 2600 mm) is adopted with a spacing of 1600 × 2400 mm and 4 bolts in each row. An anchor bolt is used along with the JSMZ20-22 new bolting device. Each bolt is anchored with 2 rolls of Z2550 resin anchor agent. The size of the bolt tray is 200 × 200 × 10 mm.

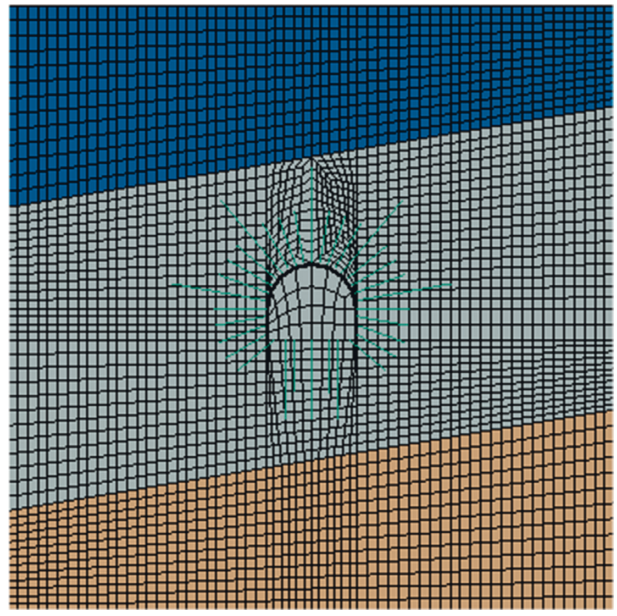

Figure 2: Grid diagram of a numerical model.

3.2.6. Floor Anchor Cable. A hollow grouting anchor cable (Φ21.6 × 4000 mm) is used with a spacing of 1600 × 2400 mm and 3 cables in each row. Each anchor cable is anchored with 3 rolls of Z2550 type resin anchor agent. The anchor cable tray is a special tray with a size of 300 × 300 × 16 mm.

Table 1: Mechanical parameters of rock strata.

Rock stratum	Elastic modulus E (GPa)	Internal friction angle φ (°)	Cohesive force c (MPa)	Poisson's ratio μ	Density ρ (kg/m^3)
Mudstone	14	32	2	0.245	2668
Siltstone	22.7	38	4	0.203	2658
Fine sandstone	43.2	35	5	0.148	2666

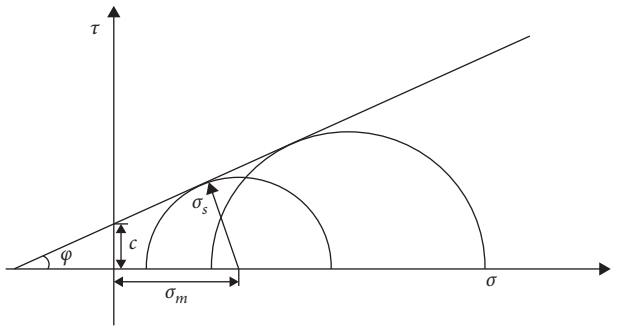

Figure 3: Illustration of Mohr–Coulomb yield criterion.

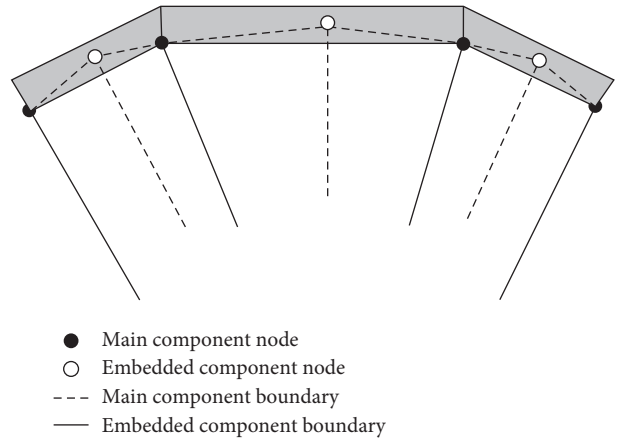

Figure 4: Distribution diagram of embedded elements.

4. Numerical Simulation of the Coupling Support

4.1. Numerical Modeling. According to the rock stratum and support parameters of the return-air roadway, a fine 2D numerical model with a size of 30×30 m has been established by the finite element software ABAQUS. From top to bottom, the rock strata with a dip angle of 10° in the model are composed by siltstone (7.5 m), mudstone (15 m), and fine sandstone (7.5 m). Both the horizontal displacement and the vertical displacement constraints are applied on the side boundaries and bottom boundaries of the numerical model. A vertical stress of 16.33 MPa calculated according to the buried depth of the model is set at the top boundary of the model. The horizontal lateral pressure coefficient is 0.8. The grid diagram of the numerical model under the initial stress state is shown in Figure 2. The mechanical parameters of rock strata are shown in Table 1.

The classic Mohr–Coulomb constitutive model [19] as shown in Figure 3 is adopted as the failure criteria of mudstone, siltstone, and fine sandstone.

The Mohr–Coulomb constitutive model can be expressed as follows:

$$\sigma_s + \sigma_m \sin \varphi - c \cos \varphi = 0, \tag{1}$$

where σ_s and σ_m are the deviating stress and the average principal stress, and they can be expressed as follows:

$$\begin{cases} \sigma_s = \dfrac{1}{2}(\sigma_1 - \sigma_3), \\ \\ \sigma_m = \dfrac{1}{2}(\sigma_1 + \sigma_3), \end{cases} \tag{2}$$

where σ_1 and σ_3 are the maximum principal stress and the minimum principal stress, respectively.

4.2. Numerical Implementation of Anchor Bolt. Shotcrete anchor support is often involved in underground projects such as tunnels, including anchoring support and lining support [20, 21]. The anchor bolt in the support system is constrained by surrounding rock and is in a tension state, so it can be simulated by rod element or beam element in finite element analysis. The "EMBEDDED" command provided by the finite element software ABAQUS can be used to simulate the interaction between the nonprestressed anchor bolt and surrounding rock, whether the anchor bolt element node coincides with the surrounding rock node or not. By using this command, the anchor bolt element can be embedded into rock elements to participate in finite element iterative calculation. The embedded instruction is to embed a specified component or a group of components into the main component, which can be used to simulate reinforcement.

The distribution of embedded elements in the main components is shown in the shaded part of Figure 4.

Generally, there are several types of embedded elements: 2D model, axisymmetric model, and 3D model. In this paper, the beam element model in the 2D model is used to realize the embedding of the anchor element, in which the interaction between bolt and surrounding rock stratum can be simulated without considering whether the embedded position structure is empty or not.

The embedded constraint has been used to define the interactions among anchor bolt and surrounding rock masses. The embedded element technique has been adopted to simulate the anchor bolt, which includes the embedded constraint. The embedded element technique can be used to model rebar reinforcement. Abaqus searches for the geometric relationships between nodes of the embedded elements (rock bolts) and the host elements (surrounding rock masses). If a node of an embedded element lies within a host element, the translational degrees of freedom at the node are eliminated and the node becomes an "embedded node." The translational degrees of freedom of the embedded node are

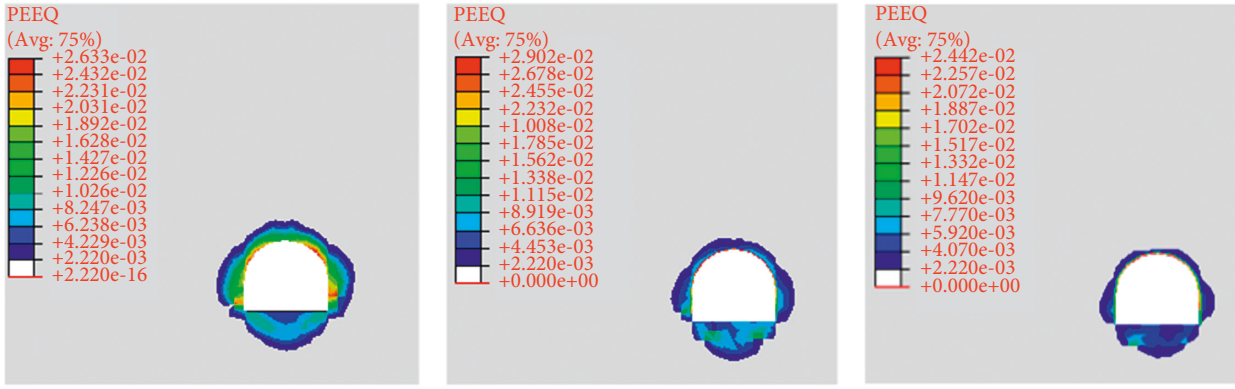

(a) (b) (c)

Figure 5: Plastic zone distribution of surrounding rock under different conditions: (a) case 1, (b) case 2, and (c) case3.

constrained to the interpolated values of the corresponding degrees of freedom of the host element. Embedded elements are allowed to have rotational degrees of freedom, but these rotations are not constrained by the embedding. Therefore, the deformation and stress of surrounding rock masses can transfer to rock bolts by the embedded element technique, which is similar to the interactions among anchor bolts and surrounding rock masses.

4.3. Analysis of Numerical Simulation Results. According to the composition of the coupling support, three cases are set as follows to analyze support response and surrounding rock response under different working conditions:

Case 1: full-section excavation without support

Case 2: full-section excavation with primary support

Case 3: full-section excavation with primary support and secondary support

The main excavation response factors, including the surface displacement of roadway, anchorage force, deep displacement of surrounding rock, and plastic zone of surrounding rock, have been analyzed under the three different cases.

4.3.1. Plastic Zone Distribution of Surrounding Rock. The plastic zone of surrounding rock can reflect the stability and safety of the roadway. Figure 5 shows the equivalent plastic strain cloud diagram of surrounding rock under three different cases, in which, PEEQ represents the value of equivalent plastic strain to reflect the cumulative result of plastic strain in the whole deformation process.

Figure 5 shows that the surrounding rock plastic zone is mainly distributed near the roadway surface, and the surrounding rock of case 1 has a larger plastic zone range compared to that of case 2 and case 3. That is to say, the application of support can effectively reduce the distribution range of the surrounding rock plastic zone. In any case, the surrounding rock plastic zone near the roadway sidewall and floor are larger than that near the roadway roof.

As shown in Figure 5(a), when the roadway is not supported, the size of the surrounding rock plastic zone near the roadway sidewall is about 30% of the roadway span, and those near the roadway floor and roof are about 56% and 27% of the roadway height. Figure 5(b), the figure of the surrounding rock plastic zone near the roadway with primary support, shows that the sizes of the surrounding rock plastic zone near the roadway sidewall and roof are significantly reduced compared with case 1, which are about 25% of the roadway span and 17% of the roadway height, respectively. However, the size of the surrounding rock plastic zone near the roadway floor is the same as in case 1. As shown in Figure 5(c), the range of the surrounding rock plastic zone further decreases after secondary support is applied, the sizes of the surrounding rock plastic zone near the roadway sidewall, floor, and roof are reduced by about 19% of the roadway span, 44%, and 10% of the roadway height. Obviously, the secondary support plays a key role in reducing the surrounding rock plastic zone.

To sum up, the application of support is helpful to reduce the surrounding rock plastic zone range and improve the stability of the surrounding rock, and the coupling support is better than the primary support alone.

Of course, Figure 5 also reflects that the maximum value of PEEQ of surrounding rock increases from 0.02633 in case 1 to 0.02902 in case 2, due to the stress concentration of surrounding rock caused by the action of the anchor bolt. Obviously, the stress concentration of surrounding rock is improved when the coupling support with a relatively dense bolt is adopted, and the maximum value of PEEQ of surrounding rock is reduced to 0.02442 in case 3.

4.3.2. Stress of Anchor Bolt and Cable. The axial stress of anchor bolts and cables under different conditions is shown in Figure 6.

Figure 6 shows that in all working conditions, the axial stress of anchor bolts and cables always decreases with the increase of the buried depth and the axial stress reaches the maximum value near the roadway surface. Obviously, this phenomenon accords with the mechanical characteristics of bonded bolts. Under the influence of the rock strata dip

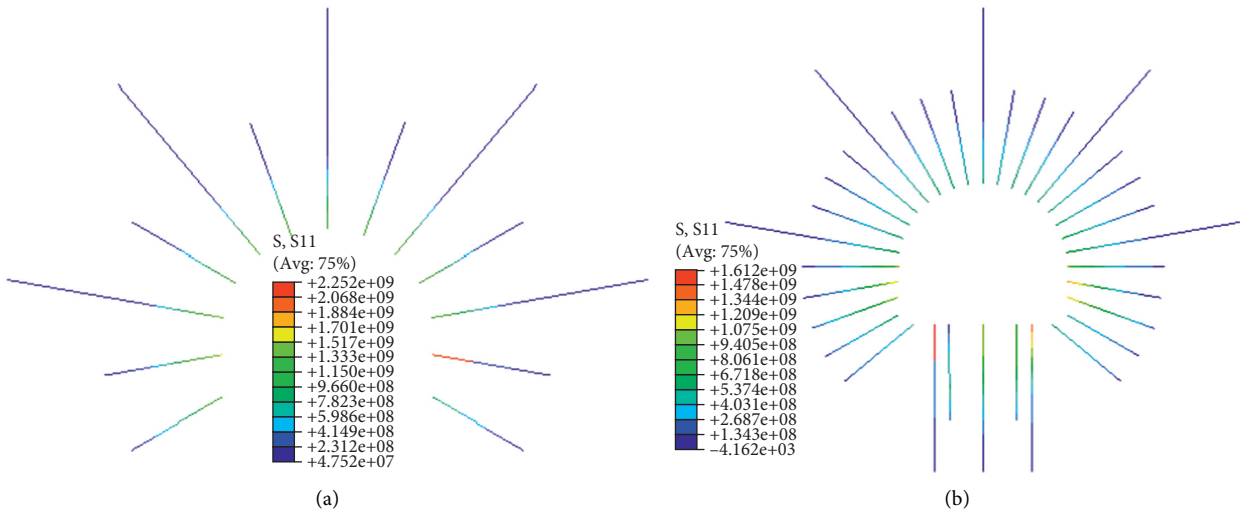

Figure 6: Axial stress clouds of anchor bolts and cables under different conditions (unit: Pa): (a) case 2 and (b) case 3.

angle, the axial stress of anchor bolts and cables arranged in different directions is different in the same buried depth.

In case 2, the maximum axial stress of anchor bolts and cables is about 2.252 GPa, which appears near the roadway sidewall. However, in case 3, the maximum axial stress of anchor bolts and cables decreases to 1.612 GPa, which appears near the roadway floor, while the maximum axial stress of bolt near the roadway sidewall is only 1.28 GPa. Obviously, the application of secondary support significantly reduces the maximum axial stress of the bolt system and changes the action mode of the bolt system. The large axial stress of the anchor bolts and cables near the roadway floor indicates that the anchor bolts and cables effectively limit the trend of floor heave and the occurrence of floor failure.

Therefore, the secondary support can change the mechanical state of surrounding rock and reduce the axial stress of anchor bolts and cables by increasing the distribution density of bolt and further improve the reliability of roadway support and the stability of surrounding rock. The coupling support can solve the problem of insufficient strength of supporting members of high-stress fractured soft rock roadway.

4.3.3. Roadway Surface Displacement. Roadway surface displacement can reflect the stability of surrounding rock and support. Therefore, as shown in Figure 7, four typical measurement points are set on roadway sidewalls, floor, and roof to carry out the comparison of roadway surface displacement under different support forms.

The roadway surface displacement under the three cases is shown in Table 2.

Table 2 shows that when the roadway is not supported, the displacement values of the four measurement points are relatively close and the maximum value appears at the roadway floor. After the application of primary support, the displacement of measurement points A, C, and D at the roadway roof and sidewall decreases rapidly by 47.3%, 28.9%, and 45.6%, respectively, while the displacement of measurement point B at the roadway floor decreases by only 4.5%. The application of secondary support further reduces the roadway surface displacement, but the measurement points with significant displacement reduction are still located at the roadway roof and sidewall. The displacement of measurement points A, C, and D decreased by 65.1%, 54.5%, and 58.2%, respectively, compared with case 1, but the measurement point D still has a small displacement change.

Therefore, the application of support can reduce the roadway surface displacement, especially the displacement

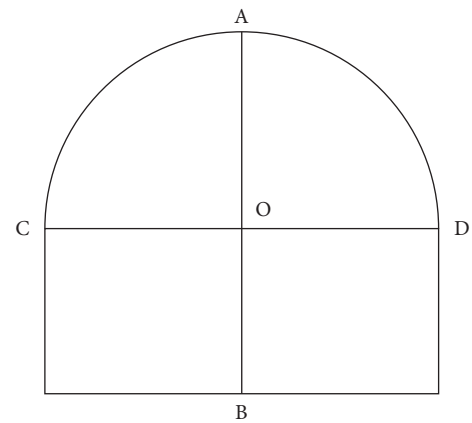

Figure 7: Surface measurement points arrangement of the roadway.

Table 2: Surface displacement of monitoring points of the roadway under different conditions.

Calculation conditions	Surface displacement of measurement points of roadway (mm)			
	A	B	C	D
Case 1	18.99	19.67	17.17	18.74
Case 2	10.00	18.79	12.21	10.20
Case 3	6.63	17.24	7.82	7.83

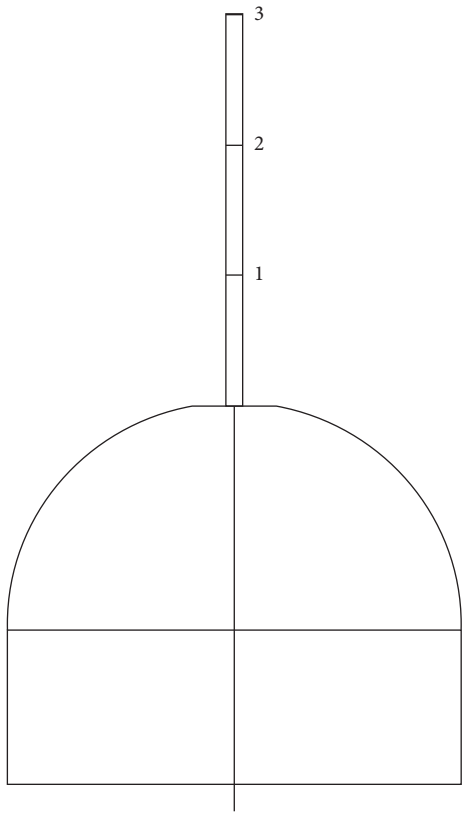

Figure 8: Measurement point for the deep displacement of surrounding rock.

at the roadway roof and sidewall. However, the effect of roadway support on inhibiting the displacement at the roadway floor is not obvious, which is basically consistent with the analysis result of inhibiting effect of roadway support on the surrounding rock plastic zone. On the whole, the coupling support has a stronger inhibition displacement ability and better supporting effect than single primary support for a high-stress fractured soft rock roadway.

4.3.4. Deep Displacement of Surrounding Rock. The deep displacement of surrounding rock is an important parameter to reflect the relaxation response and deformation law of surrounding rock induced by excavation. For the deep displacement of surrounding rock, three measurement points above the roadway roof are selected on the vertical axis of the model, numbered as 1, 2, and 3 in sequence and the distances between the measurement points and the roadway roof are 2.0 m, 5.0 m, and 8.0 m, as shown in Figure 8.

Table 3 shows the displacements of three measurement points in the surrounding rock above the roadway roof under different cases.

It can be seen from Table 3 that no matter what support method is adopted, the deep displacement of surrounding rock decreases in accordance with nonlinear law as the distance between measurement points and roadway surface increases. In case 3, the displacement of all measurement points is smaller than that in case 2, and the displacements of three measurement points are reduced by 33.2%, 17.2%, and 15.1%, respectively. That is to say, the increase of support strength caused by the application of secondary support effectively controls the deep displacement of surrounding rock and reduces the loosening range of surrounding rock.

Combined with the displacement of the roadway roof described in Table 2, the maximum relative displacement of measurement points appears between measurement point 1 and measurement point 2, so it can be considered that the main range of surrounding rock loosening does not exceed measuring point 2.

Therefore, the application of support can reduce not only the roadway surface displacement but also the deep displacement of surrounding rock. For high-stress fractured soft rock roadway, coupling support has a stronger ability to suppress deep displacement of surrounding rock than single primary support. Under the roadway support, the loosening of surrounding rock mainly occurs within 5 m from the roadway surface.

5. Support Effect Monitoring Analysis

Based on the analysis of support bearing characteristics by numerical simulation, the coupling support technology proposed in this paper is applied in the east wing return-air roadway in the Qingdong Coal Mine of Huaibei Mining Group. The applicability and reliability of the coupling support in high-stress fractured soft rock roadway are verified by field monitoring.

The measurement points of roadway surface displacement are arranged by using the cross-point method, and the location is shown in Figure 7. The spacing of measuring points along the axis of the roadway is about 30 m~40 m. 12 measurement points on 3 sections are set up during the monitoring process. The surface displacements of the roadway on the two observed sections are shown in Figure 9.

According to Figure 9, when the coupling support is done, all the displacements of measurement points are greater than the numerical simulation results. This phenomenon is mainly due to the well-known time effect [22, 23] of surrounding rock deformation, and the large time difference between support application and roadway excavation causes large initial deformation. Obviously, the influence of the time effect is difficult to predict in numerical simulation. In addition, the measured displacement of roadway floor is less than that of roadway sidewall and roof, which is opposite to the numerical simulation results. It shows that the deformation of surrounding rock near the roadway floor is less affected by time effect than that of the surrounding rock near the roadway sidewall and roof. It is beneficial and necessary to control the large deformation of surrounding rock by timely supporting following the roadway excavation.

It can be seen from Figure 9 that the deformation of all the measurement points gradually increases with time and eventually tends to a stable state, and the displacement of the roadway floor is always smaller than that of the roadway sidewall and roof. After 5 months of measurement, the maximum value of roof sinking, floor heave, and sidewall

Table 3: Deep displacement of surrounding rock under different conditions.

Calculation conditions	Displacement of roof measurement point (mm)		
	Measurement point 1	Measurement point 2	Measurement point 3
Case 2	9.52	5.46	4.82
Case 3	6.36	4.52	4.09

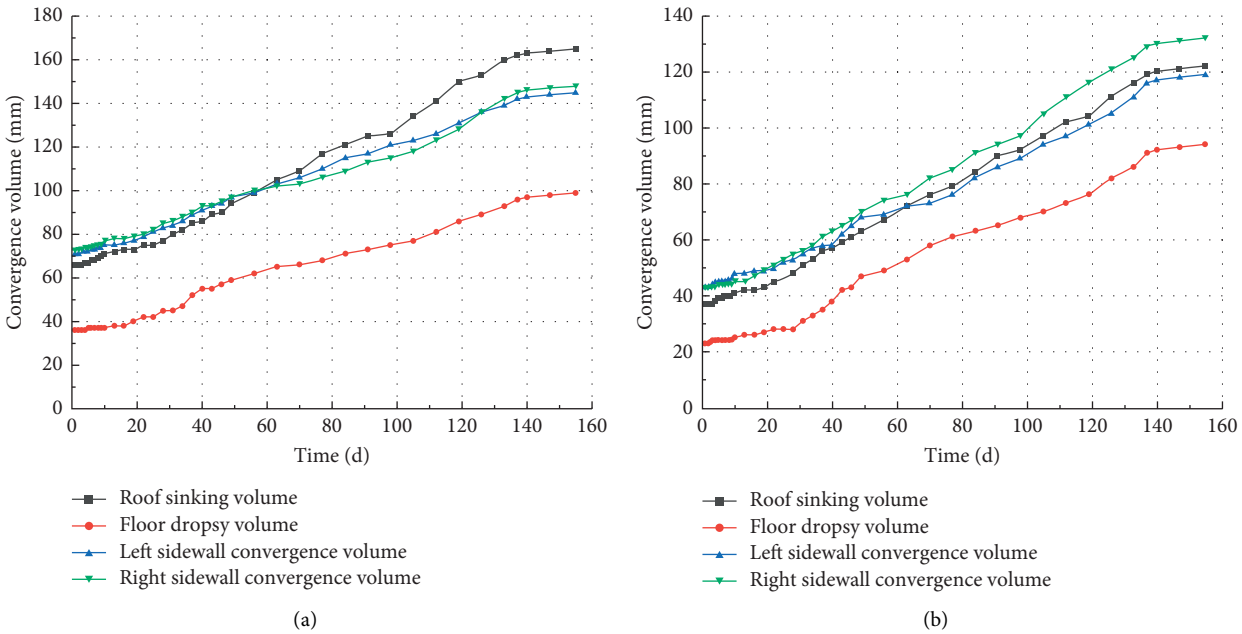

Figure 9: Convergence curve of measurement points at the return-air roadway: (a) measurement point 1 and (b) measurement point 2.

Figure 10: Support effect of the return-air roadway: (a) support effect of the roof and (b) support effect of the sidewall.

convergence of the roadway finally reached about 160 mm, 100 mm, and 150 mm, respectively. These deformation values seem to be large, but in fact, they are all within the controllable range. At the end of monitoring, the displacement of roadway support no longer increases significantly, which indicates that the deformation of surrounding rock has reached a stable state, and the deformation of surrounding rock caused by roadway excavation has been effectively controlled by the coupling support. The roadway with coupling support is shown in Figure 10.

6. Conclusions

A bolt-net-cable-grout coupling support is proposed to solve the problem in the supporting of high-stress fractured soft rock roadway. The mechanism of interaction between coupling support and surrounding rock is analyzed by numerical simulation, and the excavation responses of coupling support and surrounding rock, such as stress and displacement, are studied. Under the guidance of numerical simulation results, the coupling support is applied to an

actual roadway, and the measurement results show that the coupling support is effective. The key conclusions of the study are as follows:

(1) The surrounding rock plastic zone near the roadway sidewall and floor is larger than that near the roadway roof, and the coupling support is more effective to reduce the distribution range of the surrounding rock plastic zone than the primary support alone. In addition, the coupling support can reduce the stress concentration of surrounding rock caused by the anchor bolt.

(2) The coupling support can change the mechanical state of surrounding rock and reduce the axial stress of anchor bolts and cables by increasing the distribution density of bolt and further improve the reliability of roadway support and the stability of surrounding rock.

(3) The coupling support has a stronger inhibition displacement ability than single primary support for a high-stress fractured soft rock roadway, especially for the displacement at the roadway roof and sidewall.

(4) Coupling support can reduce not only roadway surface displacement but also deep displacement and plastic zone size of surrounding rock. For high-stress fractured soft rock roadway, the coupling support has a stronger ability to suppress the deep displacement of surrounding rock than the single support.

(5) Field monitoring data indicate that bolt-net-cable-grout coupling support changes the structure of high-stress fractured soft rock roadway and restrains the occurrence of floor heave, which proves that the comprehensive treatment of surrounding rock is effective.

Data Availability

The datasets generated and analyzed during the current study are available from the corresponding author on reasonable request.

Conflicts of Interest

The authors declare that there are no conflicts of interest.

Acknowledgments

This work was financially supported by the National Natural Science Foundation of China (No. 52074005).

References

[1] Q. H. Qian, "The current development of nonlinear rock mechanics: The mechanics problems of deep rock mass," in *Proceedings of the 8th Rock Mechanics and Engineering Conference*, pp. 10–17, Science Press, Beijing, China, 2004.

[2] M. C. He, H. P. Xie, S. P. Peng, and Y. D. Jiang, "Study of rock mechanics in deep mining," *Chinese Journal of Rock Mechanics and Engineering*, vol. 24, no. 16, pp. 2803–2813, 2005.

[3] D. F. Malan and S. M. Spottiswoode, "Time-dependent fracture zone behavior and seismicity surrounding deep level stopping operations," in *Proceedings of the Rockburst and Seismicity in Mines*, pp. 173–177, A. A. Balkema, Rotterdam, 1997.

[4] E. J. Sellers and P. Klerck, "Modelling of the effect of discontinuities on the extent of the fracture zone surrounding deep tunnels," *Tunnelling and Underground Space Technology*, vol. 15, no. 4, pp. 463–469, 2000.

[5] X. C. Kang, D. Guo, and Z. Y. Lu, "Mechanism of roadway floor heave controlled by floor corner pile in deep roadway under high horizontal stress," *Advances in Civil Engineering*, vol. 2021, pp. 1–10, Article ID 6669233, 2021.

[6] W. Zheng, Y. Zhao, Q. Bu, and S. I. Kundalwal, "The coupled control of floor heave based on a composite structure consisting of bolts and concrete antiarches," *Mathematical Problems in Engineering*, vol. 2018, Article ID 3545423, 14 pages, 2018.

[7] J. Shi and D. S. Kong, "Floor heave mechanism and anti-slide piles control technology in deep and large-span chamber," *Applied Sciences*, vol. 11, no. 10, p. 4576, 2021.

[8] Q. Wang, R. Pan, B. Jiang, S. C. Li, M. C. He, and H. B. Sun, "Study on failure mechanism of roadway with soft rock in deep coal mine and confined concrete support system," *Engineering Failure Analysis*, vol. 81, pp. 155–177, 2017.

[9] H. S. Jia, L. Y. Wang, K. Fan, B. Peng, and K. Pan, "Control technology of soft rock floor in mining roadway with coal pillar protection: A case study," *Energies*, vol. 12, no. 15, p. 3009, 2019.

[10] C. Wang, Y. P. Wu, S. J. Chen et al., "Analysis and application on inverted arch support of cross-cut floor heave," *Journal of Physics: Conference Series*, vol. 2002, no. 1, pp. 713–720, Article ID 012069, 2021.

[11] R. S. Yang, Y. L. Li, D. M. Guo et al., "Causes of deformation damage and support technology for deep high stress soft rock roadways," *Journal of Mining & Safety Engineering*, vol. 34, no. 6, pp. 1035–1041, 2017.

[12] A. Chen, X. B. Li, X. S. Liu, Y. L. Tan, K. Xu, and H. L. Wang, "Relief-retaining control technology of floor heave in mining roadway with soft rock: A case study," *Advances in Civil Engineering*, vol. 2021, Article ID 1455052, 13 pages, 2021.

[13] L. J. Zheng, Y. J. Zuo, Y. F. Hu, and W. Wu, "Deformation mechanism and support technology of deep and high-stress soft rock roadway," *Advances in Civil Engineering*, vol. 2021, Article ID 6634299, 14 pages, 2021.

[14] F. N. Wang, S. Z. Chen, P. Gao, Z. B. Guo, and Z. G. Tao, "Research on deformation mechanisms of a high geostress soft rock roadway and double-shell grouting technology," *Geofluids*, vol. 2021, Article ID 6215959, 13 pages, 2021.

[15] Q. B. Meng, L. J. Han, F. Zhang, J. Zhang, J. W. Nie, and S. Y. Wen, "Coupling support effect on high-stress deep soft rock roadway and its application," *Rock and Soil Mechanics*, vol. 38, no. 5, pp. 1234-1235+1444, 2017.

[16] P. F. Jiang, H. P. Kang, Z. G. Wang et al., "Principle, technology and application of soft rock roadway strata control by means of rock bolting, U-shaped yielding steel arches and back filling in synergy in 1 000 m deep coal mines," *Journal of China Coal Society*, vol. 45, no. 3, pp. 1020–1035, 2020.

[17] M. C. He, G. F. Zhang, G. L. Wang, Y. L. Xu, C. Z. Wu, and Q. D. Tang, "Research on mechanism and application to floor

heave control of deep gateway," *Chinese Journal of Rock Mechanics and Engineering*, vol. 28, pp. 2593–2598, 2009.

[18] L. Z. Xu and S. J. Wei, "Control technology and simulation study of floor heave in high stress soft rock roadway," *Geotechnical & Geological Engineering*, vol. 38, no. 4, pp. 4045–4058, 2020.

[19] H. W. Ma, L. Liu, P. Wang, S. Yuan, Q. R. He, and X. L. Yang, "Calculation method and mechanism of ultimate side resistance of screw pile," *Marine Georesources & Geotechnology*, vol. 2021, Article ID 2014003, 15 pages, 2021.

[20] B. Bai, R. Zhou, G. Q. Cai, W. Hu, and G. C. Yang, "Coupled thermo-hydro-mechanical mechanism in view of the soil particle rearrangement of granular thermodynamics," *Computers and Geotechnics*, vol. 137, no. 8, Article ID 104272, 2021.

[21] B. Bai, G. C. Yang, T. Li, and G. S. Yang, "A thermodynamic constitutive model with temperature effect based on particle rearrangement for geomaterials," *Mechanics of Materials*, vol. 139, Article ID 103180, 2019.

[22] L. Liu, H. W. Ma, X. L. Yang, Q. R. He, and S. Yuan, "A calculation method of bearing capacity of single squeezed branch pile based on load transfer method," *Advances in Materials Science and Engineering*, vol. 2022, pp. 1–9, Article ID 9597047, 2022.

[23] H. W. Ma, Y. Y. Wu, Y. Tong, and X. Q. Jiang, "Research on bearing theory of squeezed branch pile," *Advances in Civil Engineering*, vol. 2020, Article ID 6637261, 12 pages, 2020.